Experimental Study of Wind Load acting on Wind Turbine Nacelles

IOP Conf. Series: Journal of Physics: Conf. Series **1037** (2018) 052019 doi:10.1088/1742-6596/1037/5/052019

Experimental Study of Wind Load acting on Wind Turbine Nacelles

Jay Prakash Goit, Yifeng Liu and Takeshi Ishihara
Department of Civil Engineering, The University of Tokyo, 7-3-1 Hongo, Bunkyo-ku, Tokyo 113-8656 Japan
E-mail: jay.goit@bridge.t.u-tokyo.ac.jp

Abstract. The paper investigates wind-induced load on wind turbine nacelles through a series of wind tunnel experiments taking into account inflow turbulence and wind direction. First of all, pressure field data is collected using pressure taps distributed over the top, side and rear surfaces of the scaled nacelle model. It is observed that mean pressure distribution for nonturbulent uniform flow and turbulent shear flow cases were similar at lower yaw angle, but for higher yaw angle, pressure coefficient is smaller (more negative) close to the upstream edge when the inflow is turbulent. However, due to enhanced momentum entrainment, the streamwise extent of such strong negative pressure region is smaller. Force coefficient computed from the pressure data shows that the peak load for turbulent inflow case is significantly higher than for nonturbulent uniform inflow case. The measurement data are also used to propose models for peak factor and coefficient of variation, which can be used to estimate peak loads. The proposed models take into account both inflow turbulence and yaw misalignment, and predicted the peak force coefficients which showed satisfactory agreement with measurement. Finally, it was found that the magnitude of the load calculated by the GL guideline was satisfactory for DLC 6.1, but it was underestimated for DLC 6.2.

1. Introduction

Severe wind conditions like typhoons are responsible for extreme loading on wind turbine components including nacelles. However, while a significant number of studies have investigated loads on blades, towers and other major components of wind turbines [1–4], little attention has been devoted to the aerodynamic load on nacelles. Even the IEC guideline – the international standard for wind turbine design – does not provide any specification regarding nacelle cover design [5]. This lack of interest on the wind-induced load on nacelle may be due to its simple design and smaller contribution to the overall cost of the wind turbine. However, there has been an incident in the southern part of Japan in which nacelles of three out of six turbines were damaged during Typhoon Maemi, and the damages were attributed to the underestimation of the ultimate load during the design [6]. More recently in 2016, typhoon and extreme wind condition were responsible for partial and complete damage of several nacelle covers at Minamiosumi and Wajima wind farms in Japan [7,8]. The details of these accidents are summarized in Table 1. Considering the detrimental effect of extreme wind conditions on the nacelle cover, a thorough investigation of the wind-induced load acting on it would be crucial. In this study, an analysis of wind loads acting on turbine nacelles is conducted through wind tunnel experiments.

Nacelle essentially being a bluff body, knowledge accumulated on bluff body aerodynamics from other engineering applications, e.g., low-rise buildings, can be crucial in improving our understanding of wind loading mechanism of nacelles. Readers are referred to Holmes [9] for introductory review on bluff body aerodynamics. Nacelle aerodynamics, however, has some noticeable differences compared

to that of other bluff bodies. For instance, the ground effect with high turbulence intensities due to surface roughness is important for low-rise buildings. However, this can be neglected for nacelles, which are usually installed on high towers. Furthermore, nacelle aerodynamics is influenced by its interaction with tower and blade.

As stated earlier, studies on wind-induced loads on nacelles or studies investigating the applicability of existing design standards and design practices of nacelle are scarce. The authors are only aware of the work by Noda and Ishihara [10] who focused specifically on aerodynamic forces on nacelles. They conducted wind tunnel experiments to measure mean wind forces and local peak pressures, and reported that peak pressure coefficients specified in the design code GL Guideline[11] are smaller than those obtained from experiments. Other works have focused on the impact of blades and atmospheric turbulence on the wind speed measured at the nacelle (see e.g. [12,13]).

The aim of this work is to investigate wind loading on wind turbine nacelles through a series of wind tunnel experiments, taking into account inflow turbulence and wind direction. To this end, pressure distributions are compared for nonturbulent uniform flow and turbulent shear flow. Furthermore, wind-induced peak forces on the nacelle surfaces are assessed as a function of wind direction. The measurement data are used to propose a model for the accurate estimation of peak wind load, with the motivation that it could lead to the improvement of the guideline specifications for nacelle design.

Table 1. Summary of damages caused by extreme wind condition at three wind farms in Japan.

Wind farm	Damaged turbines	Damages	Wind condition
Miyakojima Island, Okinawa, Japan WT: 6 x (0.4 - 0.6 MW)	6	3 WTs: Collapsed completely 3 WTs: Blades and nacelle cover	Typhoon Maemi, on 11/01/2003 [6]
Minamiosumi WF, Kagoshima, Japan WT: 20 x 1.3 MW	14	7 WTs: Nacelle cover flew away 4 WTs: Inside of the nacelle 3 WTs: Radiator cover	Typhoon 16, on 20/09/2016 [7]
Wajima WF, Ishikawa, Japan WT: 5 x 600 kW	1	Nacelle cover fell	Extreme wind speed with 35.7 m/s peak value on 17/04/2016 [8]

2. Experimental setup and inflow characteristics

The experiments were conducted in the closed-circuit type boundary layer wind tunnel at The University of Tokyo. Figure 1 shows the schematic of the wind tunnel test section which has dimensions of $\mathrm{l} \times \mathrm{w} \times \mathrm{h} = 10.0 \times 1.5 \times 1.8\ \mathrm{m}^3$. As shown in the figure, combination of spires, fence and blocks were used as tripping mechanism to generate turbulence profiles. Measurements were carried-out for a nonturbulent uniform inflow (turbulence intensity 0.4%) and for shear flows with three different turbulence intensities, i.e. 4.0%, 9.2% and 13.2%, while mean velocity at the nacelle hub height was set to 13.5 m/s for all the measurements.

A single hot wire anemometer connected to Dantec Multichannel CTA 54N80, was used to measure inflow profiles at the nacelle position. Measurements were taken in the vertical direction from 0.025 m to 0.8 m at intervals of 0.08 m. Sampling rate of hot wire measurement was 1 kHz, sampling period was one minute for each height and averaging period was also one minute. Figure 2 shows the vertical profiles of the normalized mean streamwise velocity u/u_{h} and turbulence intensity $I_{\mathrm{u}} = \sigma/U$ for the nonturbulent uniform case and the shear flow case with the highest turbulence. Here, u_{h} is the mean velocity at the hub height and σ is the standard deviation. It is evident from the figure that the boundary layer height for the nonturbulent uniform flow is $z/z_{\mathrm{h}} = 0.3$, where z_{h} is the hub height of the model. The mean velocity profile for the turbulent shear flow roughly follows the power law profile given by:

$$u/u_o = (z/z_h)^{\alpha} \quad (1)$$

with exponent $\alpha = 0.2$.

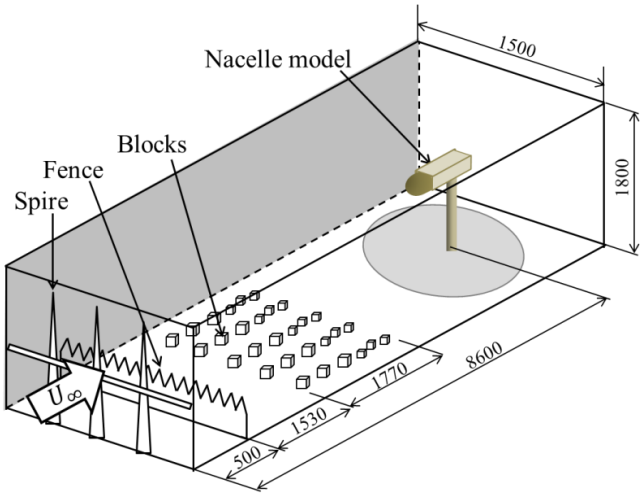

Figure 1. Schematic of wind tunnel test section showing locations of turbulence generator and nacelle model.

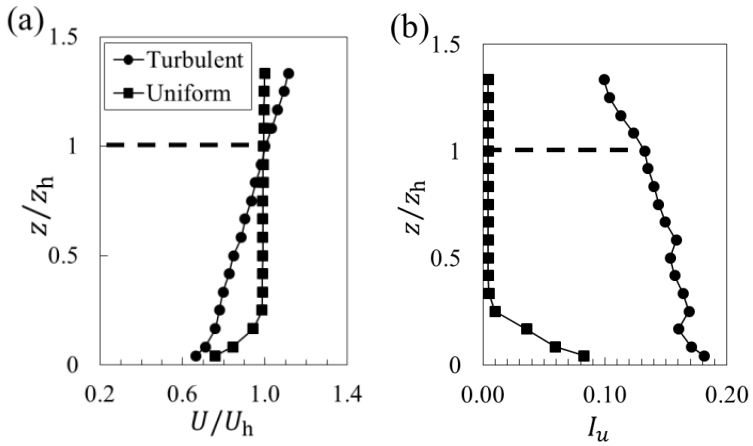

Figure 2. Vertical profiles of (a) mean velocity and (b) turbulence intensity at the position of the nacelle model.

The wind turbine nacelle model used in this study is shown in figure 3. It has dimensions of $0.2\text{m} \times 0.08\text{m} \times 0.08\text{m}$, with an additional 0.08m for the hub, and is mounted on a tower of height 0.56 m. As shown in figure 1, the nacelle model was installed on the wind tunnel turntable, which allows the yaw angle to be changed. Since the blockage ratio of the nacelle model was less than 1% for all the yaw angles, the blockage effect could be neglected in this study. Pressure data were collected using 84 pressure taps on top and side surfaces and 28 pressure taps on the rear surface (*cf.* Figure 3). Pressure transducers (Melontechnos Co., Ltd.) with range of ± 1250 Pa and sensitivity of 125 Pa/Volt were used. Sampling rate was set to 512 Hz for the current study. Pressure taps were connected to the transducers using 1.5 m long tubes with inner and outer diameters of 1 mm and 1.7 mm respectively. Prior to actual experiments, dynamic response of the tubing system was investigated by measuring its transfer function. It was found that frequencies below 55 Hz experienced amplification, while the higher frequencies experienced considerable attenuation. The distortion of the pressure signals due to the tubing was corrected using gain and phase characteristics obtained from the dynamic response investigation.

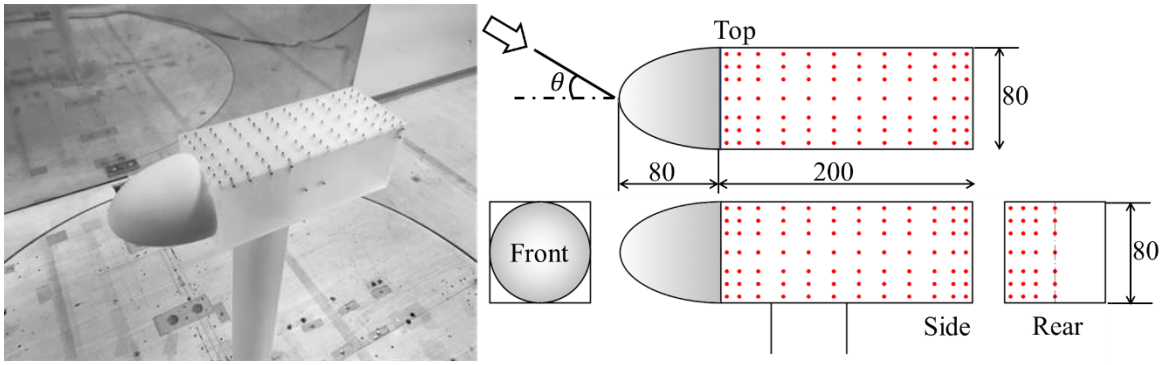

Figure 3. Design and dimensions of the nacelle model. Pressure orifices are distributed on the top, one of the sides and rear surfaces.

Table 2. Summary of the experimental cases.

Case	Inflow	Turbulence level at hub height	Yaw angle (θ)
1	Nonturbulent uniform	0.4%	0° to 355° at 5° interval
2	Turbulent shear flow	4%	$0^\circ, 15^\circ, 90^\circ, 180^\circ$
3	Turbulent shear flow	9.2%	$0^\circ, 15^\circ, 90^\circ, 180^\circ$
4	Turbulent shear flow	13.2%	0° to 355° at 5° interval

Table 2 summarizes the measurement cases, which are defined based on inflow turbulence level. Pressure measurements were conducted for yaw angle from 0° to 355° at the interval of 5° for Case 1 and Case 4. For the two intermediate cases, measurements were conducted for selected yaw angles. Note that counter clockwise direction with respect to the incident wind indicates positive yaw angle. Sampling period was one minute for each data set and five sets of data were collected for each yaw angle. Peak pressure coefficients from all five data sets were averaged to define maximum and minimum pressure coefficients at that yaw angle [10].

Since mean velocity at the nacelle hub height (U_h) was set to 13.5 m/s, the Reynolds number calculated from the U_h and the nacelle width (0.08 m) as a representative length was $Re_\mathrm{h} = 7.3 \times 10^4$. It is obvious that the Reynolds number is very much smaller than that for a typical utility-scale wind turbine of multi-megawatt capacity. The nacelle model used in the experiment is roughly 1/50 of full-scale wind turbine nacelle, and if extreme wind condition is also considered, the wind speed can be in the range of 50 m/s (4 times higher than current experiments). Thus, Reynolds number achieved in the experiment will be 1/200th of full scale. It may be of a concern that the low Reynolds number in the experiment would result in different flow separation compared to the full-scale nacelle. However, for the bluff body like nacelle, the sharp edges and corners promote separation and that is very similar to the separation for full-scale [14]. This is well accepted when investigating aerodynamics of buildings with a wind tunnel size model. Although investigating the scale effect is out of scope of this paper, additional measurements were conducted for $U_\mathrm{h} = 5.5$ m/s ($Re_\mathrm{h} = 3.0 \times 10^4$) and turbulence level of 13.2%. It was found that the difference between pressure coefficients for the two Reynolds number were negligible. Note that this justification is not quite true for the curved shape of the hub. But as it will be clear from the results, peak loads occur during yawed condition when the contribution of edges and corner on the flow structure is dominant. Therefore, this will not make the findings of this work less significant. The parameter that is indeed crucial is the inflow turbulence. Most onshore wind turbine installation sites are characterized by medium to high turbulence intensity, depending upon the topography and atmospheric condition. However, in the recent years more and more wind turbines are being installed at offshore sites which usually have lower turbulence intensity. Thus, it is necessary to consider case with different level of turbulence.

3. Result and discussions

Pressure distribution for uniform and turbulent inflow are first presented in this section. Next, wind induced forces estimated using the pressure information are discussed. Finally, models for the estimation of peak wind loads are proposed and compared against the measurements for different inflow turbulence.

3.1. Pressure field measurement

Time series of pressure data is collected for inflow conditions and yaw angles specified in table 2. The surface pressure data collected in this way can be expressed in the form of pressure coefficient:

$$C_{p,i} = \frac{(p_i - p_{\text{ref}})}{1/2\,\rho u_{\text{h}}^2} \tag{2}$$

where p_i is the measured instantaneous pressure at the pressure tap i, p_{ref} is the reference static pressure outside the influence of the nacelle model.

Figure 4 shows the mean pressure coefficient for uniform case and for turbulent boundary layer case with turbulence intensity 13.2% for yaw angles 0°, 15°, 90° and 180°. Yaw angle of 15° is also shown here because for the design load case (DLC) 6.1 in the IEC guideline, yaw misalignment of $\pm 15^\circ$ has to be considered [5]. It is observed that mean pressure coefficients are negative or close to zero for all yaw angles. But the region with negative $C_{p,\text{mean}}$ increases when yaw angle increases from 0° to 90°. This is because the sharp edge of the nacelle facing the incoming flow increases with yaw angle and as obvious, it is largest at 90°. Sharp edge is responsible for flow separation, hence increasing the region with negative pressure coefficient. But at 0°, the incoming flow greatly streamlines around the hub, thus resulting in a smaller separation region. It is further observed that $C_{p,\text{mean}}$ distribution for uniform and turbulent flow is similar for 0° yaw angle. However, conspicuous differences between uniform and turbulence inflow cases can be noticed for 90° and 180°. For both of these angles, pressure coefficient is smaller (more negative) close to the edge facing the incoming flow when the inflow is turbulent. However, the streamwise extent of this negative pressure region is smaller for turbulent inflow case. This is because the higher level turbulence enhances mixing and momentum entrainment from the free stream flow to the separation region.

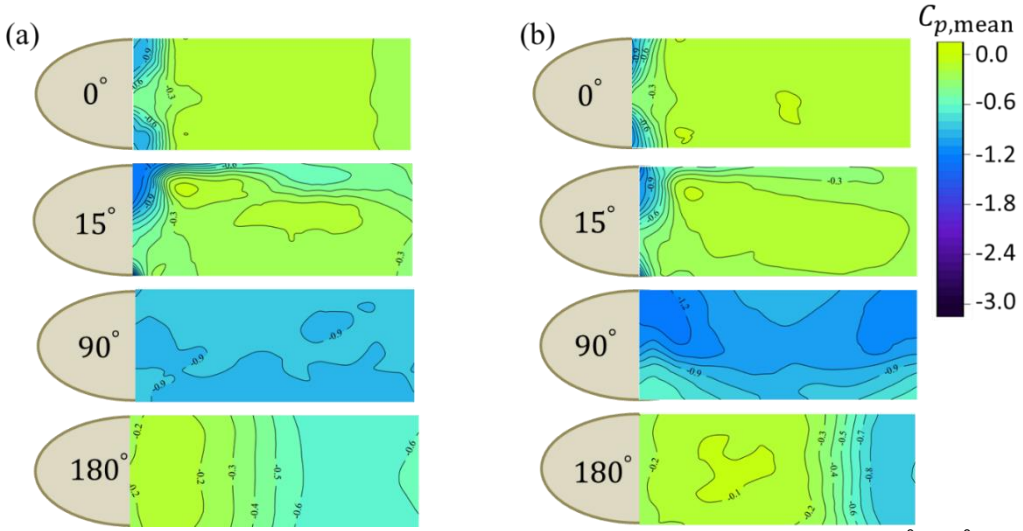

Figure 4. Contours of time-averaged pressure coefficient on the nacelle roof for 0°, 15°, 90° and 180° yaw angles. (a) Nonturbulent uniform inflow, (b) Turbulent shear inflow.

3.2. Wind load estimation

To evaluate the overall effect of wind loading, forces acting on the nacelle surfaces estimated from the pressure measurement data are analysed. As shown in figure 5, only the forces normal to the top, side

and rear surfaces are investigated in this study. To this end, point-wise pressure measurement is integrated over the particular nacelle surface. For the top surface, this force is given by:

$$F_{n,\mathrm{t}} = -\int_A p\mathrm{d}A \quad = -\sum_{i=1}^{N} p_i \mathrm{d}A_i \tag{3}$$

where p_i and $\mathrm{d}A_i$ are measured pressure and differential area of the pressure tap i. Coefficient of the force is then given by:

$$C_{Fn,\mathrm{t}} = \frac{F_{n,\mathrm{t}}}{1/2\,\rho u_{\mathrm{h}}^2 A} \tag{4}$$

where A is representative area. Vertical force $F_{n,\mathrm{t}}$, which results in the lift force on the nacelle roof, is investigated because of its possible damaging effect compared to the drag force which will not be significant. $F_{n,s}$ and $F_{n,\mathrm{b}}$ and their corresponding coefficients can be defined in the similar way.

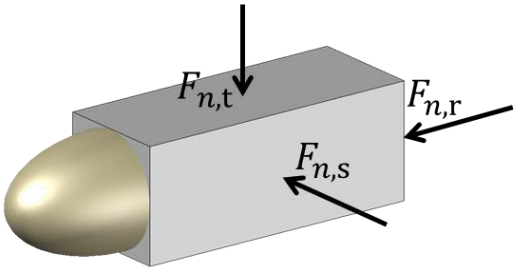

Figure 5. Schematic showing definition of normal forces and moment.

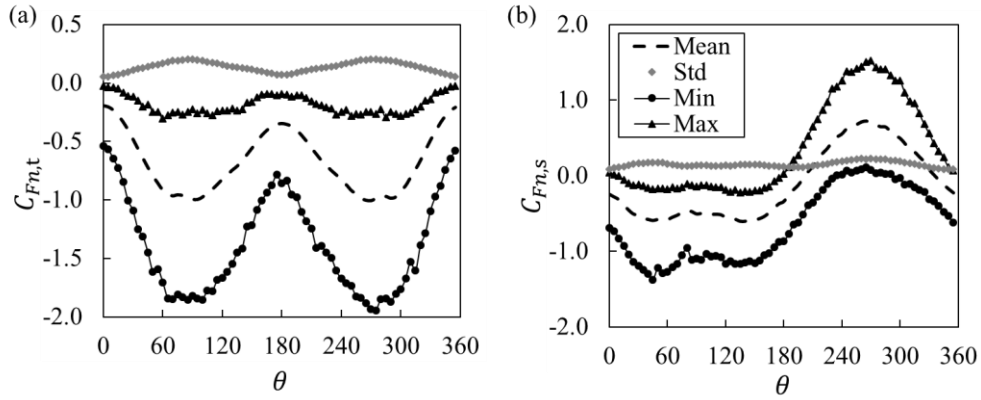

Figure 6. Forces coefficients on the (a) top and (b) side surfaces of the nacelle for inflow turbulence intensity 13.2%.

Figure 6 shows variation of the mean, minimum, maximum and standard deviation of force coefficients on the top surface and side surface as the function of yaw angle for case 4 with 13.2% turbulence intensity. For the top surface, mean, maximum and minimum force coefficients are negative for all the yaw angles. This is because the measured pressure coefficients for all the points are negative for the entire yaw angle. Consequently, the maximum force coefficient is negligibly small. On the other hand, the magnitude of minimum $C_{Fn,\mathrm{t}}$ is significantly large compared to the mean force coefficient. Two distinct peaks –around 90° and 270°– are observed for minimum and mean $C_{Fn,\mathrm{t}}$. For the side surface, the yaw angle ranges, $0^\circ \leq \theta \leq 200^\circ$ and $\theta \geq 340^\circ$ are dominated by flow separation, and therefore, it experiences outward force. This results in the larger magnitude of minimum force coefficient. For the rest of the yaw angle range, the side surface faces the incoming flow, and hence, it is pushed inward. Therefore, minimum force is negligible, while the magnitude of maximum force

coefficient is significantly higher. The maximum value of the peak force coefficient for the side surface is around 1.5. It should be noted that the magnitude of peak force coefficients on the nacelle roof is approximately 2.0, indicating that the nacelle roof experiences higher forces compared to the side surfaces.

For the comparison, mean, maximum, minimum and standard deviation of force coefficients on the top surface for the uniform inflow are shown in Figure 7. Peaks are at 60° and 300° for this case, though for yaw angle between 45° and 135° and that between 225° and 315°, variation in $C_{Fn,\mathrm{t}}$ is minimal. The difference between maximum, minimum and mean force coefficients is not too large, and the magnitudes of minimum force coefficient and standard deviation are significantly smaller compared to the turbulence inflow case in Figure 6 (a). It is apparent from this discussion that the inflow turbulence plays crucial role on nacelle aerodynamics and it particularly dictates the peak load experience by nacelles.

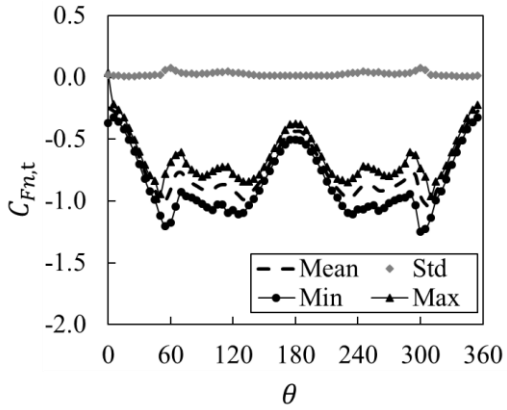

Figure 7. Force coefficients on the top surface for nonturbulent uniform inflow.

3.3. *Model for peak load estimation and comparison with measurements*

In this section, a model for estimation of peak force is proposed, following the paradigm of equivalent static wind loading (ESWL). For quasi-steady assumption the peak wind-induced force is given by [9]:

$$\hat{C}_F = \left(1 + gI_{C_F}\right)\bar{C}_F \tag{5}$$

where $\hat{C}_F$ and $\bar{C}_F$ are peak and mean force coefficients respectively and σ_{C_F} is standard deviation of the force coefficient. Peak factor g and coefficient of variation I_{C_F} is defined as:

$$\mathrm{g} = \left|\frac{\left(\hat{C}_F - \bar{C}_F\right)}{\sigma_{C_F}}\right|, \qquad I_{C_F} = \left|\frac{\sigma_{C_F}}{\bar{C}_F}\right|. \tag{6}$$

Figure 8 shows the peak factor and coefficient of variation obtained from the measurement of vertical force on the nacelle roof for case 4 (*cf.* figure 6 (a)). The values of g and I_{C_F} suggested by Noda and Ishihara [10] are also shown in the figures. It can be seen from Figure 8 (a) that the values of g obtained from the measurement are higher than the constant value proposed by Noda and Ishihara [10]. Furthermore, as discussed above, the peak forces strongly depend on inflow turbulence, indicating that g cannot have a single constant value, and should be a function of turbulence intensity. Finally, g also varies with the yaw angle (or wind direction). Considering these two factors, following model for g is proposed from the best fit to the measured value.

$$\mathrm{g} = \begin{cases} 10I_u cos\,2\theta + 5.2 & \bar{C}_F < 0 \\ 3.5 & \bar{C}_F > 0 \end{cases} \tag{7}$$

Similar to peak factor, coefficient of variation should also be a function of inflow turbulence intensity, and thus, following model for I_{C_F} is proposed. As it will be clear from the comparison below, for positive mean force coefficient existing model for g and I_{C_F} gave satisfactory result, thus they are not modified in this study.

$$I_{C_F} = \begin{cases} 0.8 \times 2I_u + 0.02 & \bar{C}_F < 0 \\ 2I_u & \bar{C}_F > 0 \end{cases} \quad (8)$$

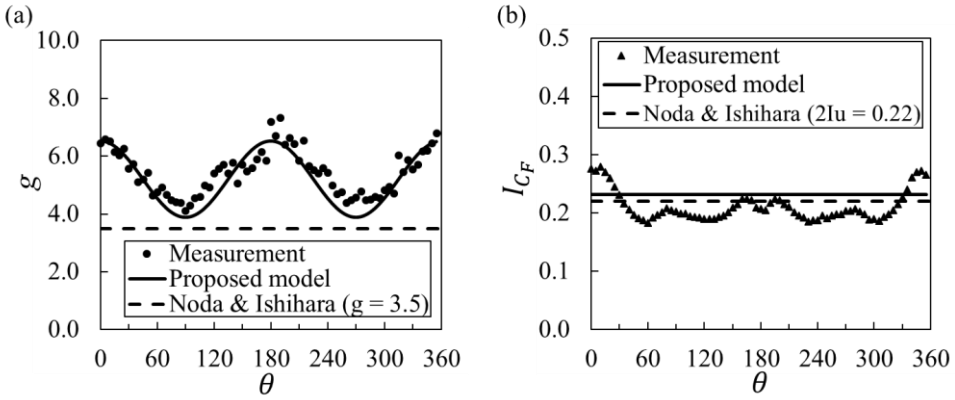

Figure 8. Measured value and model-estimated value of (a) Peak factor (g) and (b) Coefficient of variation (I_{C_F}) for turbulence intensity of 13.2%. Conventionally accepted values of g and I_{C_F} are also plotted [9].

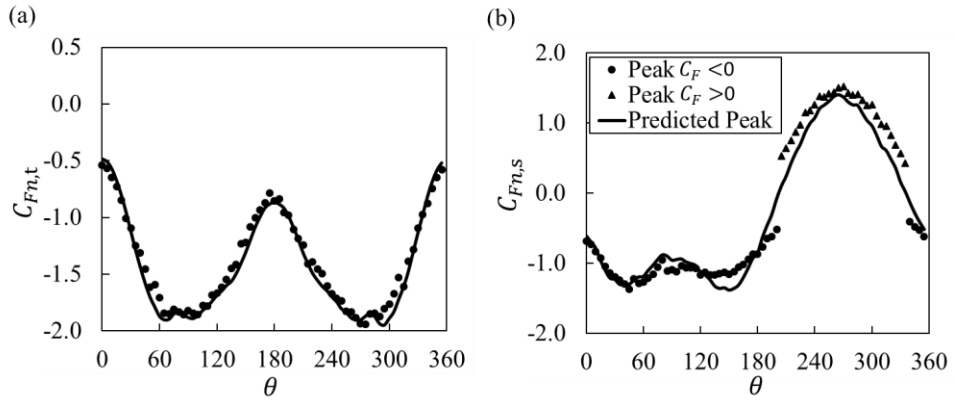

Figure 9. Comparison between predicted and measured forces coefficients on the (a) top and (b) side surfaces of the nacelle for inflow turbulence intensity 13.2%.

Figure 9 compares peak forces coefficients on the top and side surfaces estimated using proposed model for peak factor and coefficient of variation, against the measured values. The peak force coefficient for the given yaw angle is either of the maximum or minimum force coefficient, the one with higher magnitude. It can be appreciated that both measurement and the model show similar characteristics. Maximum peak values observed at 90° and 270° in the measurements are also reproduced by the model for the nacelle roof. For the reference, peak force coefficient obtained from GL guideline [11] is also shown in the figure. Note, that, the GL guideline specifies the pressure coefficient on the nacelle roof to be -0.6 for extreme wind load evaluation. As discussed further below, the guideline underestimates the peak force coefficient for a large range of yaw angle. The agreement is acceptable for side surfaces as well. The discontinuity can be observed when the peak force coefficients changes the sign for the side surface, i.e., $\theta = 200^{\circ}$ and $\theta = 335^{\circ}$. The proposed model is not able to

address this discontinuity. However, peak force is not maximum (or negative minimum) for these yaw angle, and thus the maximum force computed using the model is still relevant for the nacelle design.

In order to estimate peak wind load using Eq. (5), (7) and (8), one still needs mean force coefficient which itself is the function of mean pressure coefficient ($\bar{C}_p$). Although GL guideline specifies constant $\bar{C}_p$ values, one for each top, side, front and rear surfaces, it is obvious that $\bar{C}_p$ varies even over the surface. Therefore, in this study mean pressure coefficient distribution are proposed based on the measurement data (*cf.* figure 4) for estimating mean force coefficient for Eq. (5). Figure 10 shows the proposed mean pressure distribution for DLC 6.1 (i.e., yaw misalignment range of $\pm 15^{\circ}$) and for DLC 6.2 (i.e. yaw misalignment range of $\pm 180^{\circ}$) for nacelle roof. It should be noted that the distribution is not symmetric in figure 10 (b), because peak force occurs around 90° and the upstream edges experience lower pressure compared to their downstream counterpart.

Peak force coefficients computed using the proposed model and the proposed pressure distribution are shown as the function of inflow turbulence intensity in figure 11. The predicted values are compared against the measurement, and for the reference, force coefficients estimated from the GL guideline are also included. The model predicted coefficients are in good agreement with the measurement. It can be appreciated that the effect of inflow turbulence is well accounted for by the model. $C_{Fn,t}$ predicted by the GL guideline is sufficiently lower than the measurements and the values are conservative for DLC 6.1. However, for DLC6.2, $C_{Fn,t}$ predicted by the GL guideline is not lower enough for turbulence cases, and it is only 65% of the measurement when turbulence intensity is 13.2%.

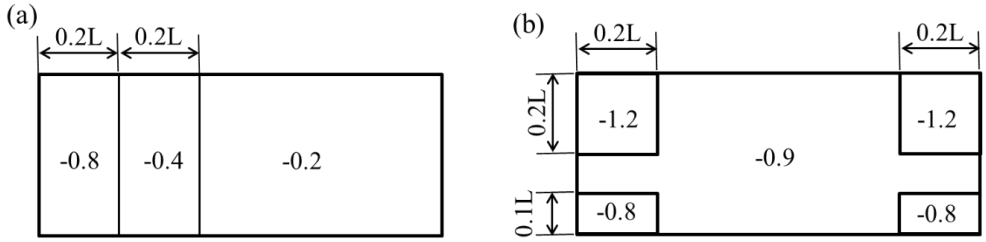

Figure 10. Mean pressure coefficient distribution proposed from the measurement. (a) For DLC 6.1, (b) for DLC 6.2.

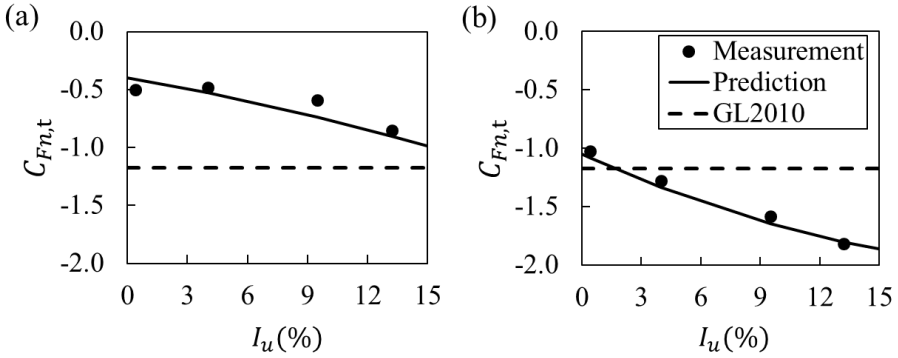

Figure 11. Variation of minimum peak force coefficients as the function of turbulence intensity. (a) $C_{Fn,\mathrm{t}}$ for DLC 6.1 and (b) $C_{Fn,\mathrm{t}}$ for DLC 6.2.

4. Conclusions

The current study investigates wind-induced load on wind turbine nacelles through wind-tunnel experiments. Pressure field data on the surface of scaled nacelle model was collected for different inflow turbulence level and analysed as the function of yaw angle. It was found that mean pressure coefficients for uniform and turbulent flow was similar for respective yaw angles. However, when the sharp edges of nacelle faces the incoming flow (for example around 90°), the mean pressure coefficient is smaller

(more negative) for the turbulence case, though due to enhanced momentum entrainment, the streamwise extent of such strong negative pressure region is smaller.

Pressure data were then integrated over the surface to evaluate wind-induced forces. It was observed that the peak forces for turbulent shear flow case were significantly higher than their nonturbulent uniform counterparts, signifying the importance inflow turbulence on the wind-induced load. Furthermore, the maximum value of peak force coefficient on the nacelle roof was higher than that on the side and rear surfaces. This indicates that nacelle roof experience higher forces compared to the side surfaces. Finally, models for the peak factor and coefficient of variation are proposed from the best fit to the measurement data. The models take into account both inflow turbulence and yaw misalignment, and predicted the peak force coefficients which showed satisfactory agreement with measurement. Finally, the load calculated by the GL guideline was sufficiently lower for DLC 6.1, but it was not lower enough for DLC 6.2, and it is only 65% of the measurement when turbulence intensity is 13.2%. Note that the Reynolds number of the current experiment was much smaller than the full scale. However, the effect of Reynolds number would be negligible for bluff bodies like nacelle, as long as the inflow turbulence level is same.

Acknowledgments
This research was carried out as a part of the project funded by Hitachi, Ltd. and ClassNK. The authors wish to express their deepest gratitude to the concerned parties for their support.

References

[1] Storey R C, Norris S E and Cater J E 2014 Modelling Turbine Loads during an Extreme Coherent Gust using Large Eddy Simulation *Journal of Physics: Conference Series* vol 524pp 1–9
[2] Freebury G and Musial W 2000 Determining equivalent damage loading for full-scale wind turbine blade fatigue tests *19th ASME Wind Energy Symposium* p 10
[3] White D L 2004 *A new method for dual-axis fatigue testing of large wind turbine blades using resonance excitation and spectral loading*
[4] Robertson A N, Wendt F, Jonkman J M, Popko W, Gueydon S, Qvist J, Vittori F, Uzunoglu E, Yde A, Galinos C, Hermans K, Bernardus J, Vaal D, Bozonnet P, Bouy L, Bayati I, Bergua R, Galvan J, Mendikoa I, Barrera C, Shin H, Molins C and Debruyne Y 2017 OC5 Project Phase II: Validation of Global Loads of the DeepCwind Floating Semisubmersible Wind Turbine *Energy Procedia* **0** 1–19
[5] IEC 61400-1 2005 *Wind turbines-Part 1: Design Requirements* vol 3
[6] Ishihara T, Yamaguchi A, Takahara K, Mekaru T and Matsuura S 2005 An Analysis of Damaged Wind Turbines by Typhoon Maemi in 2003 *The Sixth Asia-Pacific Conference on Wind Engineering* pp 1413–28
[7] Anon 2016 *Minamiosumi wind farm nacelle cover damage report (Japanese)*
[8] Anon 2016 *Wajima wind farm number 2 wind turbine nacelle cover damage report (Japanese)*
[9] Holmes J D 2015 *Wind Loading of Structures* (CRC Presee Taylor & Francis Group)
[10] Hiroshi Noda and Takeshi Ishihara 2014 Wind tunnel test on mean wind forces and peak pressures acting on wind turbine nacelles *Wind Energy* **17** 1–17
[11] Germanischer Lloyd 2010 *GL Guideline for the Certification of Wind Turbines*
[12] Zahle F and Sørensen N N 2010 Characterization of the unsteady flow in the nacelle region of a modern wind turbine *Wind Energy* **14** 271–83
[13] Masson C and Smaïli A 2006 Numerical study of turbulent flow around a wind turbine nacelle *Wind Energy* **9** 281–98
[14] Tamura Y and Kareem A 2013 *Advanced Structural Wind Engineering*